UC Davis

UC Davis Previously Published Works

Title

Low-energy collisions between electrons and BeD+

Permalink

https://escholarship.org/uc/item/2vd4z193

Journal

Plasma Sources Science and Technology, 27(2)

ISSN

0963-0252

Authors

Niyonzima, S

Pop, N

Iacob, F

et al.

Publication Date

2018

DOI

10.1088/1361-6595/aaabef

Peer reviewed

eScholarship.org Powered by the California Digital Library
University of California

Low-energy collisions between electrons and BeD^+

S. Niyonzima[1,2], N. Pop[3], F. Iacob[4], Å. Larson[5], A.E. Orel[6], J.Zs. Mezei[2,7,8], K. Chakrabarti[9], V. Laporta[2,10], K. Hassouni[7], D. Benredjem[11], A. Bultel[12], J. Tennyson[10], D. Reiter[13], I.F. Schneider[2,11]

[1]Département de Physique, Faculté des Sciences, Université du Burundi, B.P. 2700 Bujumbura, Burundi
[2]Laboratoire Ondes et Milieux Complexes CNRS−Université du Havre−Université Normandie, 76058 Le Havre, France
[3]Fundamental of Physics for Engineers Department, Politehnica University Timisoara, 300223 Timisoara, Romania
[4]West University of Timioara, Romania
[5]Department of Physics, Stockholm University, AlbaNova University Center, 106 91 Stockholm, Sweden
[6]Department of Chemical Engineering and Materials Science, University of California, Davis, California 95616, USA
[7]Laboratoire des Sciences des Procédés et des Matériaux, CNRS−Université Paris 13−USPC, 93430 Villetaneuse, France
[8]Institute of Nuclear Research, Hungarian Academy of Sciences, Debrecen, Hungary
[9]Department of Mathematics, Scottish Church College, Kolkata 700 006, India
[10]Department of Physics and Astronomy, University College London, WC1E 6BT London, UK
[11]Laboratoire Aimé-Cotton, CNRS−Université Paris-Sud−ENS Cachan−Université Paris-Saclay, 91405 Orsay, France
[12]CORIA, UMR CNRS 6614, Normanide Université, Campus Universitaire du Madrillet, 675 Avenue de l'Université, 76801 Saint-Etienne du Rouvray Cedex, FRANCE
[13]Institute of Energy and Climate Research-Plasma Physics, Forschungszentrum Jülich GmbH Association EURATOM-FZJ, Partner in Trilateral Cluster, 52425 Jülich, Germany

E-mail: `ioan.schneider@univ-lehavre.fr`

October 2017

Abstract. Multichannel quantum defect theory is applied in the treatment of the dissociative recombination and vibrational excitation processes for BeD^+ ion on its twenty four vibrational levels of its ground electronic state ($X\,^1\Sigma^+, v_i^+ = 0 \ldots 23$). Three electronic symmetries of BeH^{**} states ($^2\Pi$, $^2\Sigma^+$, and $^2\Delta$), have been employed in the calculation of cross sections and the corresponding rate coefficients. The vibrational dependence of these collisional processes is highlighted. The resulting data are useful in magnetic confinement fusion edge plasma modelling and spectroscopy, in devices with Beryllium based main chamber materials, such as ITER and JET, and operating with the deuterium-tritium fuel mix. The extensive rate coefficients database is presented in

graphical form and also by sufficiently accurate analytic fit functions which parameters being organized in tables supplied as supplementary material.

1. Introduction

The design of the International Thermonuclear Experimental Reactor (ITER) is aimed at demonstrating scientific and technological feasibility of fusion power [1]. It's now widely accepted by the fusion community that some form of controlled thermonuclear reactor, capable of producing a useful amount of electrical power, will be built-in the not-too-distant future. To obtain tenfold power multiplication in a controlled fusion process, at a power level greater than 500 megawatts and during pulses of 10 min or longer, exothermic reactions involving light nuclei, those between the hydrogen isotopes, are by far the most probable and efficient. The Joint European Torus (JET), in operation since 1983, has been persistently upgraded to become an ITER-like wall. It's the largest and most powerful tokamak in the world capable of operating with the deuterium-tritium fuel mix. One of the main improvements of JET was to equip the vessel with a first wall material combination comprising beryllium (Be) in the main chamber and tungsten (W) in the divertor [2, 3, 4]. The choice of these plasma facing components is expected to improve the machine conditioning, impact on operational space and energy confinement. The installation of Be and W in the main chamber wall of JET is aimed at studying the impurity evolution and material migration under plasma and material conditions relevant for ITER [5]. The selection of Beryllium in the main chamber wall is explained by its operational flexibility anticipated for a low-Z main wall [6], its low-fuel retention and excellent getter properties confirmed experimentally [7]. In tokamak, material erosion limits the lifetime of plasma-facing components, while in the edge and divertor regions of fusion reactors, plasma-wall interactions generate new molecular species, this formation of impurities being allowed by the relatively low-temperatures of this region of the fusion plasma. Moreover, due to the strong chemical affinity of beryllium and tungsten to oxygen, those surfaces will be oxidized [8].

In JET, the formation of BeD as well as the presence of Be, Be^+, BeD^+, BeT^+ and other impurities into the plasma are clearly described in [2, 9] and experimentally confirmed by spectroscopic methods [2, 3, 4, 10, 11, 12]. Be erosion as well as its continuous deposition towards the divertor is intrinsic to plasma operation due to the relatively high chemically assisted physical sputtering yield of Be *via* the radical BeD molecule [4] which dissociates *via* the reactions [3]:

$$e + \mathrm{BeD} \rightarrow \mathrm{Be} + \mathrm{D} + e\,. \tag{1}$$

Though deuterium ion bombardment of Be targets may cause the formation of the stable BeD_2 molecule near the main chamber, there is no spectroscopic access to the released BeD_2 molecule by chemically assisted physical sputtering of Be wall [3, 11]. Furthermore, retention of fuel elements by implantation in Be is expected to be saturated quickly due

to the narrow interaction zone [7]. With the full W divertor installed in JET, all Be ions flowing into the inner divertor [10] are originated primarily in the main chamber during diverted plasma operation. Finally, the main physics mechanism responsible for the fuel retention under the Be wall conditions in the JET experiments is co-deposition of fuel in Be co-deposits [7]. The rate of fuel retention with the ion flux to the main plasma facing components in both the divertor and main chamber is increased by co-deposition of fuel atoms with Be [6, 12]. This information is in line with the measured spectral line emission of BeII (Be^+) influx [4, 11] from the main chamber into the inner divertor whose plasma-facing surfaces are a net deposition zone [10].

In tokamaks with Be/W environment, all studies aimed at physics understanding of beryllium migration and connecting the lifetime of first wall components under erosion with tokamak safety in relation to the temporal behaviour of each fraction contribution to the long-term retention, is of great importance. The erosion mechanism itself is not studied in this work, but we are interested in data to support diagnosing beryllium in the fusion plasma. Moreover, in JET equiped with Be/W wall environment and operating with deuterium-tritium fuel mix, the rate of Be erosion is mesured by spectroscopy of all the states of the atoms and molecules, so primarily of Be, Be^+, Be_2^+, BeD, BeD^+, BeD_2, BeT, BeT^+, BeT_2, BeD_2^+ and BeT_2^+. Several observations of Be erosion by optical emission spectroscopy of various transitions of Be (at 457 nm) [2, 3], Be^+ (at 527 nm and 436nm) [3] and the BeD $A\,^2\Sigma^+ \rightarrow X\,^2\Sigma^+$ band emission (band head at 497-500 nm) [11] under different plasma conditions and surface temperatures, have been carried out successfully in laboratories and JET experiments.

Even though BeD^+ is expected to be stable in the JET divertor plasma [13], being formed through the reactions [3, 11],

$$e + \mathrm{BeD} \rightarrow \mathrm{BeD}^+ + e + e\,, \tag{2}$$

$$\mathrm{Be}^+ + \mathrm{D}_2 \rightarrow \mathrm{BeD}^+ + \mathrm{D}\,, \tag{3}$$

its $A\,^1\Sigma^+ \rightarrow X\,^1\Sigma^+$ band emission in visible and ultra-violet range is not observable, due to its probable weak intensities [13, 14], BeD and BeD^+ being the only beryllium hydride molecules released in the plasma [2]. Therefore, Be is the main and dominant intrinsic impurity in limited and diverted plasmas with the JET. Those impurities hugely influence the low temperature edge and divertor plasma behaviour in which electrons and ions originating from the core plasma are cooled by radiation and charge exchange processes till below 1 eV [1, 15, 16]. All molecular species in these regions undergo many collisions, particularly those between electrons and molecular ions [15]. The electron-impact processes of vibrationally excited BeD^+ play a key role in the reaction kinetics of low-temperature plasmas in general, and particularly also in certain cold regions of fusion reactor relevant (*e.g.* the divertor) plasmas. Hence, modelling and diagnosing these varied plasma environments require accurate, reliable cross-sections and rate coefficients for interactions of these molecular ions with electrons [17] which produce simpler species, most of which being unsuitable for visible spectroscopy. This complete database of cross-sections and rate coefficients for electron-impact collision

processes coupled to the availability of absolutely calibrated spectroscopic emission from this molecular ion provide a way to characterise also the BeD$^+$ formation rates in the edge and divertor plasma of fusion devices.

This work is a part of a series of papers [9, 18, 19] devoted to the study of electron-impact processes in fusion devices with beryllium-based main chamber materials. We present reactive collisions cross sections and rate coefficients between electrons and the BeD$^+$ molecular ion in all vibrationnal states, relevant for the divertor and edge plasma kinetics of JET and ITER. In collision with electrons the BeD$^+$ ion undergoes several processes, in particular dissociative recombination (DR) and vibrational-excitation/de-excitation (VE/VdE), respectively [20, 21]:

$$e + \mathrm{BeD}^+(v_i^+) \rightarrow \mathrm{Be} + \mathrm{D}\,, \qquad \text{(DR)} \tag{4}$$

$$e + \mathrm{BeD}^+(v_i^+) \rightarrow \mathrm{BeD}^+(v_f^+) + \mathrm{e}^-\,, \qquad \text{(VE/VdE)} \tag{5}$$

where $v_i^+(v_f^+)$ denoting the initial(final) vibrational level of the cation. The process of dissociative excitation will be discussed in a future paper.

The manuscript is organized as follows: In Section 2, we briefly review the theoretical method used to calculate the cross sections and the corresponding rate coefficients; Section 3 presents Maxwellian isotropic rate coefficients computed for the DR, VE and VdE processes. These rate coefficients have been fitted with a modified Arrhenius law. Section 4 contains the final remarks concluding the paper.

2. Brief description of the theoretical approach of the dynamics

In the present paper, we used the Multichannel Quantum Defect Theory (MQDT)-type approach to study the vibrational resolved reactive collisions of beryllium deuteride cation (BeD$^+$) with electrons. We assumed BeD$^+$ initially in its electronic ground state, X $^1\Sigma^+$, of energies below the dissociation limit of the target. The electron-impact collision processes covered by the present article involve two mechanisms which are treated simultaneously by the MQDT [22]: (i) the *direct* process, in which the electron is captured into a doubly excited resonant state BeD** of the neutral system, resulting in two neutral atomic fragments Be and D or in autoionization,

$$e + \mathrm{BeD}^+(v_i^+) \rightarrow \mathrm{BeD}^{**} \rightarrow \begin{cases} \mathrm{Be} + \mathrm{D} \\ \mathrm{BeD}^+(v_f^+) + e\,, \end{cases} \tag{6}$$

and (ii) the *indirect* process consisting in the temporary capture of the electron into BeD*, a singly excited bound Rydberg state, predissociated by BeD**,

$$e + \mathrm{BeD}^+(v_i^+) \rightarrow \mathrm{BeD}^* \rightarrow \mathrm{BeD}^{**} \rightarrow \begin{cases} \mathrm{Be} + \mathrm{D} \\ \mathrm{BeD}^+(v_f^+) + e\,. \end{cases} \tag{7}$$

In MQDT approach, the processes (i) and (ii) result in the total mechanism by quantum interference. As mentionned in Eqs. (6) and (7), the excited neutral system, reached by the electron capture, can autoionize to the initial electronic state of a different vibrational quantum number v_f^+ and then expel an electron to the continuum.

Vibrational excitation takes place when $v_f^+ > v_i^+$, while vibrational de-excitation occurs if $v_f^+ < v_i^+$. The quantum defect approach treats the processes represented by Eqs. (6) and (7) as multichannel reactive processes involving the dissociation channels (accounting for the atom-atom scattering) and ionization channels (accounting for the electron-molecular ion scattering). Each ionization channel, for which the collision coordinate is the electron distance r from the molecular ion center, is defined by its threshold, a vibrational level v^+ of the molecular ion ground state and by the angular quantum number l of the incoming or outgoing electron. An ionisation channel is open if its corresponding threshold is situated below the total energy of the system, and closed in the opposite case. This later channel introduces in the calculations a series of Rydberg states differing only by the principal quantum number of the external electron [23]. Complementary, a dissociation channel, having the internuclear distance R as the collision coordinate, relies on an electronically bound state BeD** whose potential energy in the asymptotic limit is situated below the total energy of the system.

As a matter of the fact, BeH$^+$ and BeD$^+$ ions having the same electronic structure, we used the same set of potential energy curves, electronic couplings [21] and quantum defects as in our previous work on BeH$^+$ [9, 19], taking care to consider the reduced mass of BeD$^+$. Moreover, as a matter of the fact the mathematical model is the same, we skip any further details and we refer to the previous article [9].

Once the scattering matrix S for the processes DR and VE/VdE are determined, the corresponding global cross sections, as a function of the incident electron kinetic energy ε, are obtained by summation over all relevant symmetries of the system and over the projection of the total electronic angular momentum on the nuclear axes Λ of the resulting partial cross sections capture into all the dissociative states d_j of the same symmetry:

$$\sigma_{diss\leftarrow v_i^+}(\varepsilon) = \frac{\pi}{4\varepsilon} \sum_{\Lambda,sym} \rho^{sym,\Lambda} \sum_{l,j} \left| S_{d_j,lv_i^+} \right|^2 , \tag{8}$$

$$\sigma_{v_f^+\leftarrow v_i^+}(\varepsilon) = \frac{\pi}{4\varepsilon} \sum_{\Lambda,sym} \rho^{sym,\Lambda} \sum_{l,l'} \left| S_{l'v_f^+,lv_i^+} - \delta_{l'l}\delta_{v_i^+v_f^+} \right|^2 , \tag{9}$$

where $\rho^{sym,\Lambda}$ is the multiplicity ratio between the electronic states of BeD and the electronic states of BeD$^+$. In order to obtain the thermal rate coefficients, we have convoluted the global cross sections with the Maxwellian distribution function for velocities v (related to incident energy of the electrons by $\varepsilon = \frac{1}{2}mv^2$) of the free electrons:

$$\alpha(T) = \frac{8\pi}{(2\pi kT)^{3/2}} \int_0^{+\infty} \sigma(\varepsilon)\, \varepsilon\, \exp(-\varepsilon/kT)\, d\varepsilon\,, \tag{10}$$

where $\sigma(\varepsilon)$ is the cross sections given by (8) or (9), k and T being the Boltzman constant and the absolute temperature respectively.

v^+	ϵ_{v^+}(eV)	v^+	ϵ_{v^+}(eV)
0	0.000	12	1.920
1	0.194	13	2.031
2	0.380	14	2.135
3	0.564	15	2.232
4	0.742	16	2.321
5	0.914	17	2.401
6	1.079	18	2.473
7	1.238	19	2.535
8	1.391	20	2.585
9	1.537	21	2.623
10	1.674	22	2.655
11	1.802	23	2.678

Table 1. BeD$^+$ vibrational levels referred to $v^+ = 0$. The values of dissociating energies are $D_e = 2.794$ eV and $D_0 = 2.682$ eV.

3. Results

Using the available molecular data - quasi-diabatic potential energy curves and electronic couplings for $^2\Pi$, $^2\Sigma^+$ and $^2\Delta$ states displayed in Figure 1 of [19] (for more details see as well [21, 24]) - we have extended our previous calculations, initially restricted to the ground and weakly excited vibrational states, to all vibrational levels (up to $v_i^+ = 23$) of the ground electronic state. Table 1 shows the list of vibrational levels of BeD$^+$ and the values of D_e and D_0. In the following calculations, the energy of the electron is inferior to 2.7 eV, this value corresponding to the dissociation threshold of the ground electronic state of the ion.

Figures 1–4 give the whole ensemble of rate coefficients available for the state-to-state kinetics of BeD$^+$. They illustrate the dominance of the DR in its $v_i^+ = 0 - 9$ levels at low electron temperature, while the VdE becomes more important than the other processes for initial vibrational states $v_i^+ > 9$. Figure 5 provides the comparison between the DR rate coefficients and the global - *i.e.* coming from the sum over all the possible final levels - vibrational transitions rate coefficients. One may notice that the excitation process becomes a notable competitor to DR and VdE above 1000 K only.

In order to allow the versatile implementation of the rate coefficients shown in Figs. 1-4 in kinetics modelling codes, we have fitted them with generalized Arrhenius-type formulas. The calculated DR rate coefficients of BeD$^+$ in each of its first 24 vibrational states ($v_i^+ = 0 \ldots 23$) have been interpolated under the mathematical form:

$$k_{v_i^+}^{DR}(T_e) = A_{v_i^+}\, T_e^{\alpha_{v_i^+}}\, \exp\left[-\sum_{j=1}^{7} \frac{B_{v_i^+}(j)}{j\; T_e^j}\right], \qquad (11)$$

over the electron temperature range $100 \leq T_e \leq 5000$ K. The values calculated by Eq. (11) depart from the referenced values only of a few percent. The parameters $A_{v_i^+}$,

$\alpha_{v_i^+}$ and $B_{v_i^+}(j)$ are listed in the Table 2. The calculated VE and VdE rate coefficients of BeD$^+$ have been interpolated under the form:

$$k^{VE,VdE}_{v_i^+ \to v_f^+}(T_e) = A_{v_i^+ \to v_f^+} \, T_e^{\alpha_{v_i^+ \to v_f^+}} \, \exp\left[- \sum_{j=1}^{7} \frac{B_{v_i^+ \to v_f^+}(j)}{j \; T_e^j} \right] , \qquad (12)$$

over the electron temperature range $300 \leq T_e \leq 5000$ K. The values calculated by Eq. (12) depart from the referenced values only of a few percent. The parameters $A_{v_i^+ \to v_f^+}$, $\alpha_{v_i^+ \to v_f^+}$ and $B_{v_i^+ \to v_f^+}(j)$ are listed in the Table 3 for the monoquantic VE. The full set of coefficients for DR, VE and VdE are given in the supplementary material of the present article.

4. Conclusions

The present paper provides a complete state-to-state rate constants of the BeD$^+$ reactive collisions with electrons, illustrating quantitatively the competition between the vibrational transitions and dissociative recombination. We display the Maxwell rate coefficients for the molecular ion in all of its initial vibrational states and for the entire range of energies of the incident electron below the ion dissociation threshold. Arrhenius-type formulas are used in order to fit the rate coefficients as function of the electron temperature. These rate coefficients strongly depend on the initial vibrational level of the molecular ion.

These data are addressed to the fusion community - being relevant to the modeling of the edge of the fusion plasma as well as for divertor conditions - and, more generally, to the modelers of any beryllium-containing-plasmas, produced in laboratory experiments, industrial processing and natural environments. No experimental work concerning the electron/BeD$^+$ collisions can be found in the literature. Further studies, devoted to higher energy and consequently taking into account the dissociative excitation [18, 25], as well as others, extending to isotopes of BeH$^+$ (BeD$^+$, BeT$^+$) are the object of ongoing work. All these data, as well as the presently displayed ones will be of huge importance for modeling of the plasma/wall interaction [26].

Acknowledgments

The authors acknowledge the French LabEx EMC^3, *via* the projects PicoLIBS (No. ANR-12-BS05-0011-01) and EMoPlaF. The BIOENGINE project (sponsored by the European fund FEDER and the French CPER), the Fédération de Recherche Fusion par Confinement Magnétique - ITER and the European COST Program CM1401 (Our Astrochemical History). AEO acknowledges support from the National Science Foundation, Grant No PHY-11-60611. In addition some of this material is based on work done while AEO was serving at the NSF. ÅL acknowledges support from the Swedish Research council, Grant No. 2014-4164. NP and SI acknowledge the Sectoral Operational Programme Human Resources Development (SOP HRD), ID134378 financed from the European Social Fund and by the Romanian Government.

References

[1] A. W. Kleyn, N. J. Lopes Cardozo and U. Samm, Phys. Chem. Chem. Phys. 8(2006) 17611774.

[2] G. Duxbury, M.F. Stamp and H.P. Summers, Plasma Phys. Control. Fusion 40 361-370 (1998).

[3] S. Brezinsek, M.F. Stamp, D. Nishijima, D. Borodin, S. Devaux, K. Krieger, S. Marsen, M. OMullane, C. Bjoerkas, A. Kirschner and JET EFDA contributors, Nucl. Fusion 54 (2014) 103001 (11pp).

[4] S. Brezinsek, A. Widdowson, M. Mayer, V. Philipps, P. Baron-Wiechec, J.W. Coenen, K. Heinola, A. Huber, J. Likonen, P. Petersson, M. Rubel, M.F. Stamp, D. Borodin, J.P. Coad, A.G. Carrasco, A. Kirschner, S. Krat, K. Krieger, B. Lipschultz, Ch. Linsmeier, G.F. Matthews, K. Schmid and JET contributors, Nucl. Fusion 55 (2015) 063021 (10pp).

[5] J.W. Coenen, M. Sertoli, S. Brezinsek, I. Coffey, R. Dux, C. Giroud, M. Groth, A. Huber, D. Ivanova, K. Krieger, K. Lawson, S. Marsen, A. Meigs, R. Neu, T. Puetterich, G.J. van Rooij, M.F. Stamp and JET-EFDA Contributors, Nucl. Fusion 53 (2013) 073043.

[6] G.F. Matthews, JET EFDA Contributors, the ASDEX-Upgrade Team, J. Nucl. Mater. 438 (2013) S2-S10.

[7] S. Brezinsek, T. Loarer, V. Philipps, H.G. Esser, S. Grnhagen, R. Smith, R. Felton, J. Banks, P. Belo, A. Boboc, J. Bucalossi, M. Clever, J.W. Coenen, I. Coffey, S. Devaux, D. Douai, M. Freisinger, D. Frigione, M. Groth, A. Huber, J. Hobirk, S. Jachmich, S. Knipe, K. Krieger, U. Kruezi, S. Marsen, G.F. Matthews, A.G. Meigs, F. Nave, I. Nunes, R. Neu, J. Roth, M.F. Stamp, S. Vartanian, U. Samm and JET EFDA contributors, Nucl. Fusion 53 (2013) 083023 (13pp).

[8] V. Kh. Alimov, Physica Scripta. Vol. T108 (2004), 4656.

[9] S. Niyonzima, S. Ilie, N. Popa, J. Zs. Mezei, K. Chakrabarti, V. Morel, B. Peres, D.A. Little, K. Hassouni, . Larson, A.E. Orel, D. Benredjem, A. Bultel, J. Tennyson, D. Reiter, I.F. Schneider, At. Data Nucl. Data T. (2016), http://dx.doi.org/10.1016/j.adt.2016.09.002.

[10] K. Krieger, S. Brezinsek, M. Reinelt, S.W. Lisgo, J.W. Coenen, S. Jachmich, S. Marsen, A. Meigs, G. van Rooij, M. Stamp, O. van Hoey, D. Ivanova, T. Loarer, V. Philipps, and JET EFDA contributors, J. Nucl. Mater. 438 (2013) S262S266.

[11] D. Nishijima, R. P. Doerner, M. J. Baldwin, G. De Temmerman and E. M. Hollmann, Plasma Phys. Control. Fusion 50 (2008) 125007.

[12] R.P. Doerner, M.J. Baldwin, D. Buchenauer, G. De Temmerman, D. Nishijima, J. Nucl. Mater.390-391(2009) 681.

[13] J.A. Coxon and R. Colin, J. Mol. Spectrosc. 181, 215-223 (1997).

[14] P. G. Koontz, Phys. Rev. 48 (1935) 707-713.

[15] G.M. McCracken, M.F. Stamp, R.D. Monk, A.G. Meigs, J. Lingertat, R. Prentice, A. Starling, R.J. Smith and A. Tabasso,Nucl. Fus. 38(1998) 619.

[16] S. I. Krasheninnikov, Physica. Scripta (2002) T96, 7-15.

[17] R. CELIBERTO, R. K. JANEV, A. LARICCHIUTA, M. CAPITELLI, J. M. WADEHRA and D. E. ATEMS, Atom. Data Nucl. Data Tabl. 77 (2001) 161213.

[18] V Laporta, K Chakrabarti, R Celiberto, R K Janev, J Zs Mezei, S Niyonzima, J Tennyson, and I F Schneider. *Plasma Physics and Controlled Fusion*, 59(4):045008, 2017.

[19] S. Niyonzima, F. Lique, K. Chakrabarti, Å. Larson , A. E. Orel, and I. F. Schneider, Phys. Rev. A 87 (2013) 022713.

[20] I. F. Schneider, O. Dulieu, and J. Robert (editors), EPJ Web of Conferences 84 (2015) (Proceedings of the 9^{th} International Conference 'Dissociative Recombination: Theory, Experiment and Applications', Paris, July 7-12 2013).

[21] J. B. Roos , M. Larsson, Å. Larson, and A. E. Orel, Phys. Rev. A 80 (2009) 012501.

[22] A. Giusti, J. Phys. B 13 (1980) 3867.

[23] Schneider I F, Dulieu O, Giusti-Suzor A, and Roueff E 1994, Astrophys. J. **424**, 983.

[24] C. Strömholm, I. F. Schneider, G. Sundström, L. Carata, H. Danared, S. Datz, O. Dulieu, A.

Källberg, M. af Ugglas, X. Urbain, V. Zengin, A. Suzor-Weiner, and M. Larson, Phys. Rev. A 52 (1995) R4320.

[25] K. Chakrabarti, D. R. Backodissa-Kiminou, N. Pop, J. Zs. Mezei, O. Motapon, F. Lique, O. Dulieu, A. Wolf and I. F. Schneider, Phys. Rev. A **87** (2013) 022702.

[26] R. Celiberto, R. K. Janev, and D. Reiter, Plasma Phys. Control. Fusion 54 (2012) 035012.

Table 2. List of the parameters used in Eq.(11) for the DR rate coefficients of BeD^+.

v_i^+	$A_{v_i^+}$	$\alpha_{v_i^+}$	$B_{v_i^+}(1)$	$B_{v_i^+}(2)$	$B_{v_i^+}(3)$	$B_{v_i^+}(4)$	$B_{v_i^+}(5)$	$B_{v_i^+}(6)$	$B_{v_i^+}(7)$
0	0.8974×10^{-09}	0.3841	$-0.2563 \times 10^{+04}$	$0.2470 \times 10^{+07}$	$-0.1130 \times 10^{+10}$	$0.2766 \times 10^{+12}$	$-0.3713 \times 10^{+14}$	$0.2571 \times 10^{+16}$	$-0.7179 \times 10^{+17}$
1	0.6299×10^{-06}	−0.2688	$-0.2190 \times 10^{+02}$	$-0.3068 \times 10^{+06}$	$0.2394 \times 10^{+09}$	$-0.7544 \times 10^{+11}$	$0.1177 \times 10^{+14}$	$-0.9028 \times 10^{+15}$	$0.2710 \times 10^{+17}$
2	0.1395×10^{-04}	−0.5889	$0.7304 \times 10^{+03}$	$-0.7024 \times 10^{+06}$	$0.3170 \times 10^{+09}$	$-0.7705 \times 10^{+11}$	$0.1032 \times 10^{+14}$	$-0.7156 \times 10^{+15}$	$0.2002 \times 10^{+17}$
3	0.3307×10^{-05}	−0.4462	$0.9445 \times 10^{+02}$	$-0.8147 \times 10^{+05}$	$0.3345 \times 10^{+08}$	$-0.7925 \times 10^{+10}$	$0.1074 \times 10^{+13}$	$-0.7665 \times 10^{+14}$	$0.2216 \times 10^{+16}$
4	0.4349×10^{-05}	−0.4673	$0.2376 \times 10^{+03}$	$-0.2605 \times 10^{+06}$	$0.1310 \times 10^{+09}$	$-0.3448 \times 10^{+11}$	$0.4893 \times 10^{+13}$	$-0.3541 \times 10^{+15}$	$0.1023 \times 10^{+17}$
5	0.2623×10^{-04}	−0.6473	$0.1421 \times 10^{+04}$	$-0.1540 \times 10^{+07}$	$0.7367 \times 10^{+09}$	$-0.1848 \times 10^{+12}$	$0.2520 \times 10^{+14}$	$-0.1766 \times 10^{+16}$	$0.4973 \times 10^{+17}$
6	0.3822×10^{-04}	−0.6855	$0.7458 \times 10^{+03}$	$-0.5492 \times 10^{+06}$	$0.1993 \times 10^{+09}$	$-0.4139 \times 10^{+11}$	$0.4962 \times 10^{+13}$	$-0.3181 \times 10^{+15}$	$0.8418 \times 10^{+16}$
7	0.6649×10^{-05}	−0.5080	$0.2471 \times 10^{+03}$	$-0.4732 \times 10^{+06}$	$0.2797 \times 10^{+09}$	$-0.7808 \times 10^{+11}$	$0.1134 \times 10^{+14}$	$-0.8287 \times 10^{+15}$	$0.2402 \times 10^{+17}$
8	0.7614×10^{-05}	−0.5318	$0.4697 \times 10^{+03}$	$-0.5195 \times 10^{+06}$	$0.2456 \times 10^{+09}$	$-0.6106 \times 10^{+11}$	$0.8275 \times 10^{+13}$	$-0.5776 \times 10^{+15}$	$0.1623 \times 10^{+17}$
9	0.6493×10^{-05}	−0.5295	$0.5057 \times 10^{+03}$	$-0.6108 \times 10^{+06}$	$0.3022 \times 10^{+09}$	$-0.7682 \times 10^{+11}$	$0.1054 \times 10^{+14}$	$-0.7416 \times 10^{+15}$	$0.2094 \times 10^{+17}$
10	0.3819×10^{-05}	−0.4877	$0.4455 \times 10^{+03}$	$-0.6156 \times 10^{+06}$	$0.3269 \times 10^{+09}$	$-0.8697 \times 10^{+11}$	$0.1230 \times 10^{+14}$	$-0.8836 \times 10^{+15}$	$0.2532 \times 10^{+17}$
11	0.2883×10^{-05}	−0.4686	$0.4699 \times 10^{+03}$	$-0.6798 \times 10^{+06}$	$0.3766 \times 10^{+09}$	$-0.1028 \times 10^{+12}$	$0.1479 \times 10^{+14}$	$-0.1074 \times 10^{+16}$	$0.3105 \times 10^{+17}$
12	0.2315×10^{-05}	−0.4563	$0.4047 \times 10^{+03}$	$-0.6130 \times 10^{+06}$	$0.3466 \times 10^{+09}$	$-0.9566 \times 10^{+11}$	$0.1385 \times 10^{+14}$	$-0.1011 \times 10^{+16}$	$0.2931 \times 10^{+17}$
13	0.1442×10^{-05}	−0.4155	$0.2709 \times 10^{+03}$	$-0.4825 \times 10^{+06}$	$0.2839 \times 10^{+09}$	$-0.8004 \times 10^{+11}$	$0.1174 \times 10^{+14}$	$-0.8643 \times 10^{+15}$	$0.2521 \times 10^{+17}$
14	0.9694×10^{-06}	−0.3803	$0.1729 \times 10^{+03}$	$-0.3907 \times 10^{+06}$	$0.2413 \times 10^{+09}$	$-0.6932 \times 10^{+11}$	$0.1026 \times 10^{+14}$	$-0.7602 \times 10^{+15}$	$0.2226 \times 10^{+17}$
15	0.7270×10^{-06}	−0.3590	$0.1667 \times 10^{+03}$	$-0.4139 \times 10^{+06}$	$0.2543 \times 10^{+09}$	$-0.7253 \times 10^{+11}$	$0.1068 \times 10^{+14}$	$-0.7881 \times 10^{+15}$	$0.2301 \times 10^{+17}$
16	0.4768×10^{-06}	−0.3232	$0.1124 \times 10^{+03}$	$-0.3870 \times 10^{+06}$	$0.2458 \times 10^{+09}$	$-0.7065 \times 10^{+11}$	$0.1042 \times 10^{+14}$	$-0.7692 \times 10^{+15}$	$0.2245 \times 10^{+17}$
17	0.3339×10^{-06}	−0.2965	$0.8587 \times 10^{+02}$	$-0.3909 \times 10^{+06}$	$0.2567 \times 10^{+09}$	$-0.7453 \times 10^{+11}$	$0.1104 \times 10^{+14}$	$-0.8167 \times 10^{+15}$	$0.2387 \times 10^{+17}$
18	0.2383×10^{-06}	−0.2735	$0.1221 \times 10^{+03}$	$-0.4597 \times 10^{+06}$	$0.2953 \times 10^{+09}$	$-0.8485 \times 10^{+11}$	$0.1250 \times 10^{+14}$	$-0.9205 \times 10^{+15}$	$0.2683 \times 10^{+17}$
19	0.1868×10^{-06}	−0.2609	$0.1973 \times 10^{+03}$	$-0.5555 \times 10^{+06}$	$0.3423 \times 10^{+09}$	$-0.9644 \times 10^{+11}$	$0.1404 \times 10^{+14}$	$-0.1025 \times 10^{+16}$	$0.2974 \times 10^{+17}$
20	0.1332×10^{-06}	−0.2495	$0.2343 \times 10^{+03}$	$-0.6118 \times 10^{+06}$	$0.3644 \times 10^{+09}$	$-0.1009 \times 10^{+12}$	$0.1454 \times 10^{+14}$	$-0.1056 \times 10^{+16}$	$0.3048 \times 10^{+17}$
21	0.1114×10^{-06}	−0.2452	$0.2826 \times 10^{+03}$	$-0.6493 \times 10^{+06}$	$0.3776 \times 10^{+09}$	$-0.1035 \times 10^{+12}$	$0.1486 \times 10^{+14}$	$-0.1076 \times 10^{+16}$	$0.3102 \times 10^{+17}$
22	0.8079×10^{-07}	−0.2366	$0.2937 \times 10^{+03}$	$-0.6480 \times 10^{+06}$	$0.3747 \times 10^{+09}$	$-0.1027 \times 10^{+12}$	$0.1475 \times 10^{+14}$	$-0.1069 \times 10^{+16}$	$0.3084 \times 10^{+17}$
23	0.4801×10^{-07}	−0.2398	$0.3455 \times 10^{+03}$	$-0.7133 \times 10^{+06}$	$0.4152 \times 10^{+09}$	$-0.1148 \times 10^{+12}$	$0.1659 \times 10^{+14}$	$-0.1208 \times 10^{+16}$	$0.3498 \times 10^{+17}$

Table 3. List of the parameters used in Eq.(12) for the monoquantic VE, $v_i^+ \to v_f^+ = v_i^+ + 1$, rate coefficients of BeD$^+$.

v_i^+	$A_{v_i^+\to v_f^+}$	$\alpha_{v_i^+\to v_f^+}$	$B_{v_i^+\to v_f^+}(1)$	$B_{v_i^+\to v_f^+}(2)$	$B_{v_i^+\to v_f^+}(3)$	$B_{v_i^+\to v_f^+}(4)$	$B_{v_i^+\to v_f^+}(5)$	$B_{v_i^+\to v_f^+}(6)$	$B_{v_i^+\to v_f^+}(7)$
0	$0.232 \times 10^{+02}$	$-0.210 \times 10^{+01}$	$0.168 \times 10^{+05}$	$-0.156 \times 10^{+08}$	$-0.611 \times 10^{+10}$	$0.173 \times 10^{+14}$	$-0.101 \times 10^{+17}$	$0.251 \times 10^{+19}$	$-0.230 \times 10^{+21}$
1	0.395×10^{-09}	$0.361 \times 10^{+00}$	$-0.592 \times 10^{+03}$	$0.698 \times 10^{+07}$	$-0.787 \times 10^{+10}$	$0.442 \times 10^{+13}$	$-0.128 \times 10^{+16}$	$0.176 \times 10^{+18}$	$-0.830 \times 10^{+19}$
2	0.156×10^{-11}	$0.887 \times 10^{+00}$	$-0.423 \times 10^{+04}$	$0.126 \times 10^{+08}$	$-0.135 \times 10^{+11}$	$0.833 \times 10^{+13}$	$-0.294 \times 10^{+16}$	$0.551 \times 10^{+18}$	$-0.424 \times 10^{+20}$
3	0.240×10^{-06}	$-0.294 \times 10^{+00}$	$0.638 \times 10^{+04}$	$-0.158 \times 10^{+08}$	$0.216 \times 10^{+11}$	$-0.150 \times 10^{+14}$	$0.567 \times 10^{+16}$	$-0.110 \times 10^{+19}$	$0.867 \times 10^{+20}$
4	0.109×10^{-07}	0.162×10^{-01}	$0.249 \times 10^{+04}$	$-0.457 \times 10^{+07}$	$0.739 \times 10^{+10}$	$-0.555 \times 10^{+13}$	$0.218 \times 10^{+16}$	$-0.439 \times 10^{+18}$	$0.353 \times 10^{+20}$
5	0.432×10^{-08}	0.776×10^{-01}	$-0.205 \times 10^{+04}$	$0.113 \times 10^{+08}$	$-0.144 \times 10^{+11}$	$0.960 \times 10^{+13}$	$-0.351 \times 10^{+16}$	$0.669 \times 10^{+18}$	$-0.519 \times 10^{+20}$
6	0.517×10^{-08}	0.507×10^{-01}	$-0.211 \times 10^{+04}$	$0.892 \times 10^{+07}$	$-0.100 \times 10^{+11}$	$0.639 \times 10^{+13}$	$-0.229 \times 10^{+16}$	$0.435 \times 10^{+18}$	$-0.336 \times 10^{+20}$
7	0.753×10^{-08}	-0.187×10^{-02}	$-0.107 \times 10^{+04}$	$0.714 \times 10^{+07}$	$-0.824 \times 10^{+10}$	$0.509 \times 10^{+13}$	$-0.175 \times 10^{+16}$	$0.318 \times 10^{+18}$	$-0.236 \times 10^{+20}$
8	0.128×10^{-07}	-0.677×10^{-01}	$-0.679 \times 10^{+03}$	$0.444 \times 10^{+07}$	$-0.448 \times 10^{+10}$	$0.262 \times 10^{+13}$	$-0.889 \times 10^{+15}$	$0.160 \times 10^{+18}$	$-0.119 \times 10^{+20}$
9	0.220×10^{-06}	$-0.353 \times 10^{+00}$	$0.627 \times 10^{+03}$	$0.160 \times 10^{+07}$	$-0.141 \times 10^{+10}$	$0.746 \times 10^{+12}$	$-0.234 \times 10^{+15}$	$0.402 \times 10^{+17}$	$-0.290 \times 10^{+19}$
10	0.143×10^{-05}	$-0.530 \times 10^{+00}$	$0.138 \times 10^{+04}$	$0.943 \times 10^{+05}$	$0.135 \times 10^{+09}$	$-0.209 \times 10^{+12}$	$0.107 \times 10^{+15}$	$-0.249 \times 10^{+17}$	$0.220 \times 10^{+19}$
11	0.380×10^{-05}	$-0.613 \times 10^{+00}$	$0.172 \times 10^{+04}$	$-0.627 \times 10^{+06}$	$0.732 \times 10^{+09}$	$-0.503 \times 10^{+12}$	$0.195 \times 10^{+15}$	$-0.394 \times 10^{+17}$	$0.321 \times 10^{+19}$
12	0.850×10^{-05}	$-0.673 \times 10^{+00}$	$0.196 \times 10^{+04}$	$-0.135 \times 10^{+07}$	$0.151 \times 10^{+10}$	$-0.976 \times 10^{+12}$	$0.358 \times 10^{+15}$	$-0.693 \times 10^{+17}$	$0.547 \times 10^{+19}$
13	0.144×10^{-04}	$-0.718 \times 10^{+00}$	$0.216 \times 10^{+04}$	$-0.203 \times 10^{+07}$	$0.230 \times 10^{+10}$	$-0.148 \times 10^{+13}$	$0.542 \times 10^{+15}$	$-0.104 \times 10^{+18}$	$0.824 \times 10^{+19}$
14	0.129×10^{-04}	$-0.698 \times 10^{+00}$	$0.192 \times 10^{+04}$	$-0.167 \times 10^{+07}$	$0.184 \times 10^{+10}$	$-0.114 \times 10^{+13}$	$0.404 \times 10^{+15}$	$-0.755 \times 10^{+17}$	$0.578 \times 10^{+19}$
15	0.160×10^{-04}	$-0.719 \times 10^{+00}$	$0.193 \times 10^{+04}$	$-0.204 \times 10^{+07}$	$0.237 \times 10^{+10}$	$-0.153 \times 10^{+13}$	$0.556 \times 10^{+15}$	$-0.106 \times 10^{+18}$	$0.827 \times 10^{+19}$
16	0.153×10^{-04}	$-0.723 \times 10^{+00}$	$0.181 \times 10^{+04}$	$-0.207 \times 10^{+07}$	$0.247 \times 10^{+10}$	$-0.161 \times 10^{+13}$	$0.591 \times 10^{+15}$	$-0.113 \times 10^{+18}$	$0.893 \times 10^{+19}$
17	0.103×10^{-04}	$-0.700 \times 10^{+00}$	$0.153 \times 10^{+04}$	$-0.162 \times 10^{+07}$	$0.189 \times 10^{+10}$	$-0.121 \times 10^{+13}$	$0.434 \times 10^{+15}$	$-0.817 \times 10^{+17}$	$0.630 \times 10^{+19}$
18	0.784×10^{-05}	$-0.691 \times 10^{+00}$	$0.137 \times 10^{+04}$	$-0.150 \times 10^{+07}$	$0.176 \times 10^{+10}$	$-0.113 \times 10^{+13}$	$0.405 \times 10^{+15}$	$-0.765 \times 10^{+17}$	$0.589 \times 10^{+19}$
19	0.401×10^{-05}	$-0.638 \times 10^{+00}$	$0.942 \times 10^{+03}$	$-0.839 \times 10^{+06}$	$0.939 \times 10^{+09}$	$-0.576 \times 10^{+12}$	$0.199 \times 10^{+15}$	$-0.365 \times 10^{+17}$	$0.276 \times 10^{+19}$
20	0.323×10^{-05}	$-0.609 \times 10^{+00}$	$0.779 \times 10^{+03}$	$-0.786 \times 10^{+06}$	$0.904 \times 10^{+09}$	$-0.574 \times 10^{+12}$	$0.205 \times 10^{+15}$	$-0.387 \times 10^{+17}$	$0.298 \times 10^{+19}$
21	0.273×10^{-05}	$-0.573 \times 10^{+00}$	$0.600 \times 10^{+03}$	$-0.489 \times 10^{+06}$	$0.528 \times 10^{+09}$	$-0.319 \times 10^{+12}$	$0.109 \times 10^{+15}$	$-0.200 \times 10^{+17}$	$0.150 \times 10^{+19}$
22	0.221×10^{-05}	$-0.545 \times 10^{+00}$	$0.446 \times 10^{+03}$	$-0.367 \times 10^{+06}$	$0.403 \times 10^{+09}$	$-0.250 \times 10^{+12}$	$0.878 \times 10^{+14}$	$-0.162 \times 10^{+17}$	$0.123 \times 10^{+19}$

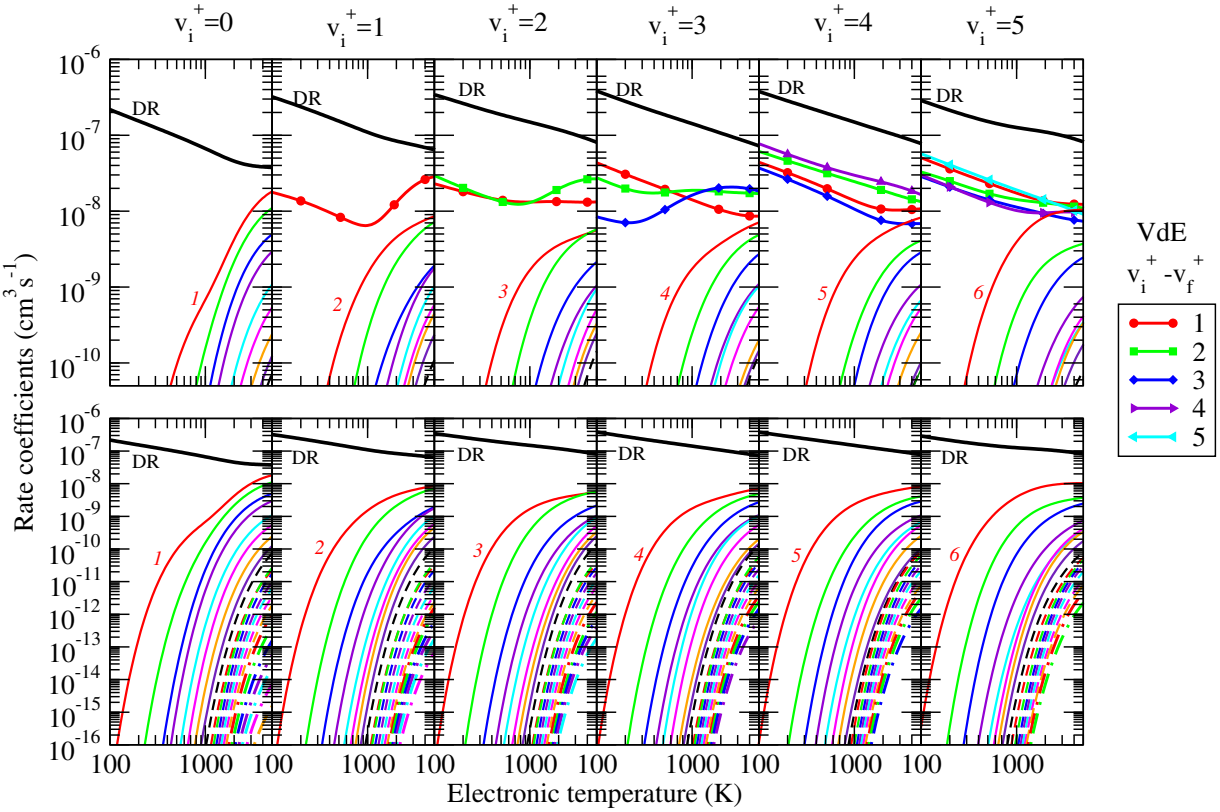

Figure 1. Dissociative recombination (DR, black line), vibrational excitation (VE, thin lines) and vibrational de-excitation (VdE, symbols and thick lines) rate coefficients of ground ($v_i^+ = 0$) and excited ($v_i^+ = 1, ..., 5$) BeD^+ in its electronic ground state (total mechanism). For VE, since the rate coefficients decrease monotonically with the excitation, the lowest final vibrational quantum number of the target is indicated only, and the lower panels extend the range down to 10^{-16} cm^3/s.

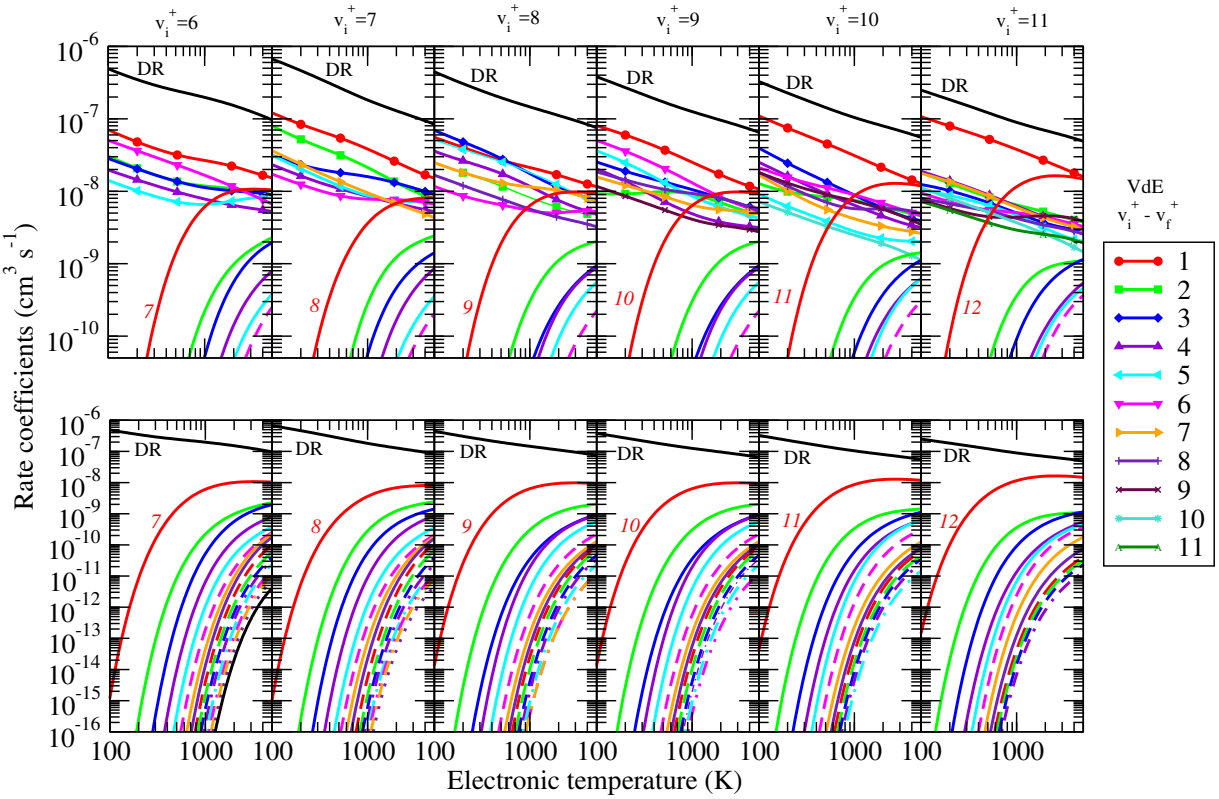

Figure 2. Dissociative recombination (DR, black line), vibrational excitation (VE, thin lines) and vibrational de-excitation (VdE, symbols and thick lines) rate coefficients of excited ($v_i^+ = 6, 7, 8, ..., 11$) BeD$^+$ in its electronic ground state (total mechanism). For VE, since the rate coefficients decrease monotonically with the excitation, the lowest final vibrational quantum number of the target is indicated only, and the lower panels extend the range down to 10^{-16} cm^3/s.

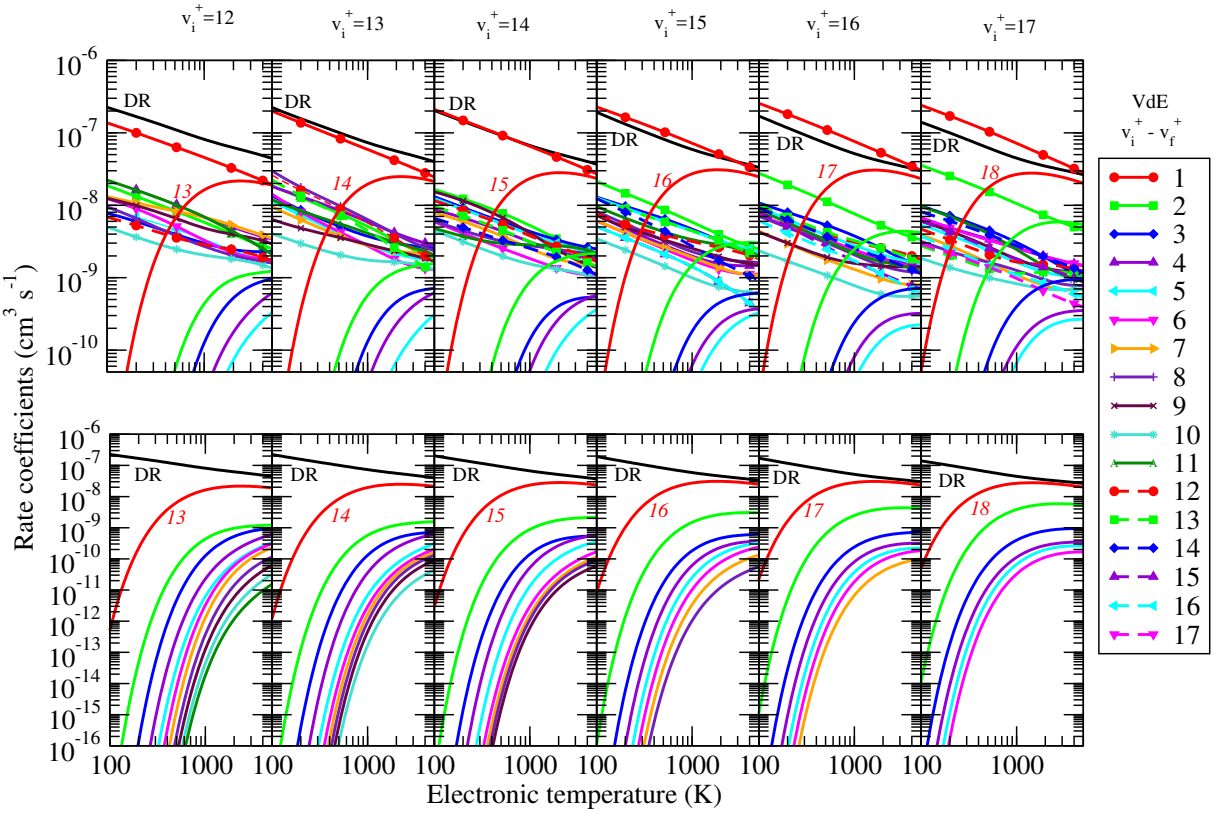

Figure 3. Dissociative recombination (DR, black line), vibrational excitation (VE, thin lines) and vibrational de-excitation (VdE, symbols and thick lines) rate coefficients of excited ($v_i^+ = 12, 13, ..., 17$) BeD$^+$ in its electronic ground state (total mechanism). For VE, since the rate coefficients decrease monotonically with the excitation, the lowest final vibrational quantum number of the target is indicated only, and the lower panels extend the range down to 10^{-16} cm^3/s.

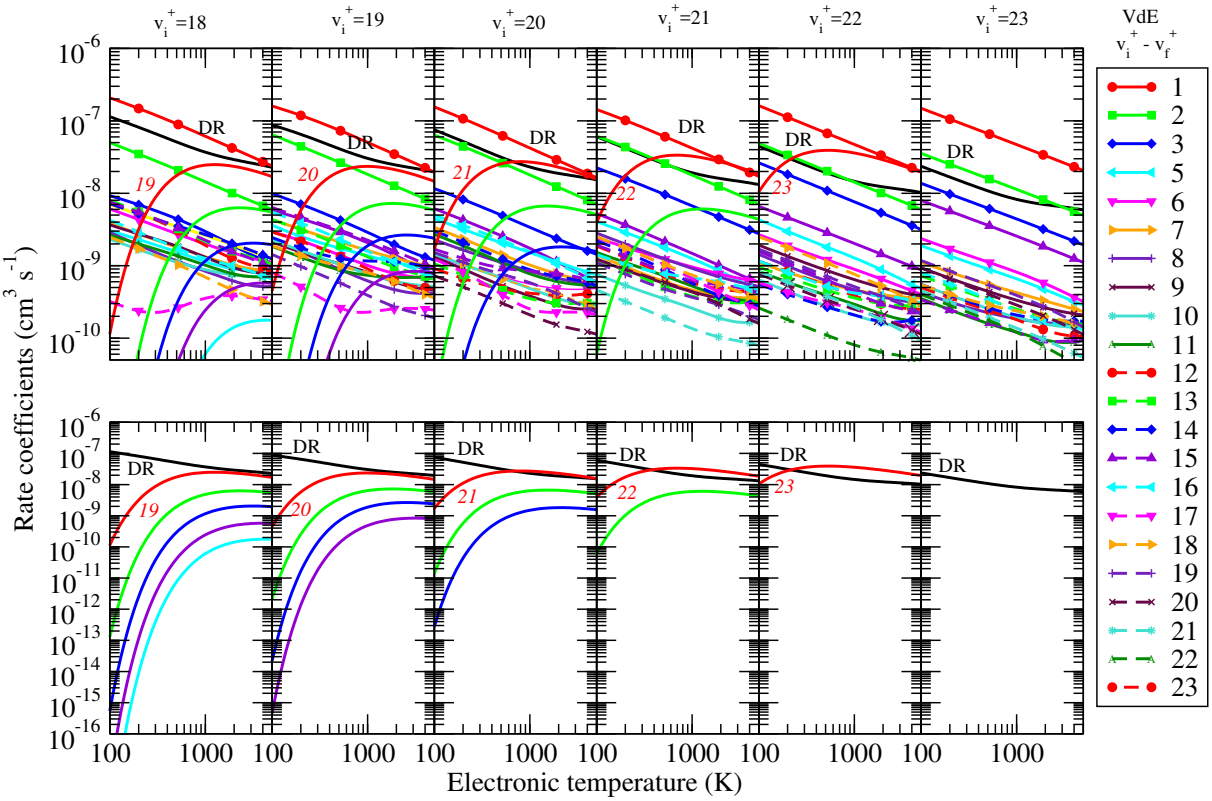

Figure 4. Dissociative recombination (DR, black line), vibrational excitation (VE, thin lines) and vibrational de-excitation (VdE, symbols and thick lines) rate coefficients of excited ($v_i^+ = 18, 19, ..., 23$) BeD$^+$ in its electronic ground state (total mechanism). For VE, since the rate coefficients decrease monotonically with the excitation, the lowest final vibrational quantum number of the target is indicated only, and the lower panels extend the range down to 10^{-16} cm^3/s.

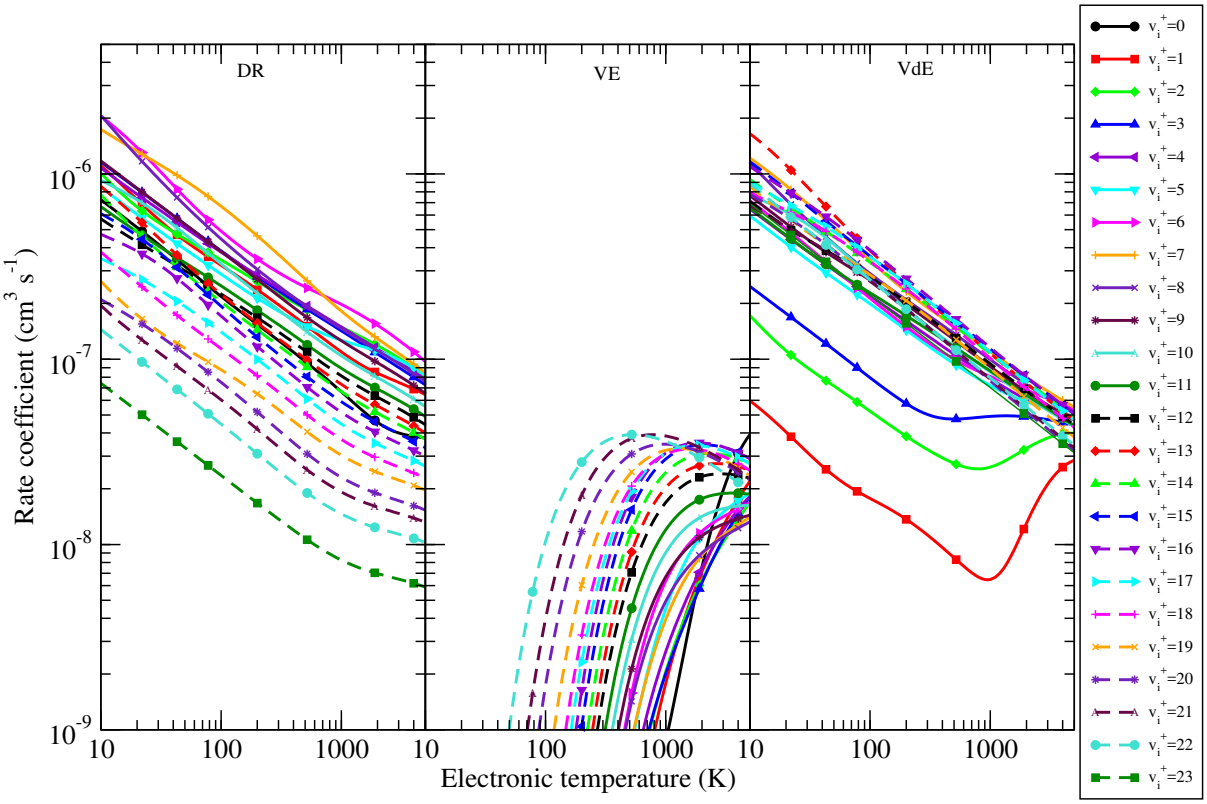

Figure 5. Global (sum over all the possible final states) rate coefficients for dissociative recombination (DR), vibrational excitation (VE) and vibrational de-excitation (VdE).